New algorithms and error analysis for sinusoidal phase shifting interferometry

Peter J. de Groot* and Leslie L. Deck
Zygo Corporation
Laurel Brook Road, Middlefield, CT 06455

ABSTRACT

An alternative to the conventional linear phase shift in optical testing interferometers is a sinusoidal phase shift, which has the benefit of relaxing requirements on the phase-shifting mechanism. We propose error-compensating phase-demodulation algorithms and provide a new, comprehensive sensitivity analyses to random noise, nonlinearity, vibrations and calibration error to demonstrate that sinusoidal phase shifting can be as robust and computationally efficient as the more established linear phase-shift techniques.

Keywords: Phase shifting, interferometry, optical testing

1. INTRODUCTION

Optical surface profilers such as the familiar laser Fizeau interferometer sketched in Figure 1 measure surface heights from an estimation of the phase profile of the wavefront reflected from the object surface.

In phase shifting interferometry or PSI, several patterns are acquired in sequence during a controlled overall phase shift to facilitate the phase estimation. By far the most common method of PSI involves a linear phase shift, which generates an oscillating intensity signal with a carrier frequency proportional to the phase shifting rate. The phase of this carrier is the phase that we seek. The importance of PSI techniques and their >20-year history for gold-standard metrology has led to highly-refined techniques and hundreds of papers on error analysis and PSI algorithm design [1].

The linear phase shift nonetheless presents some challenges and limitations, particularly with regard to the phase shifting mechanism. Mechanical shifting is the most common method, using piezo-electric actuators or the like, driving optical sub assemblies that can weigh several pounds or more. Because these actuators have limited range, they can maintain the phase shift for just a few interference intensity cycles before reversing direction.

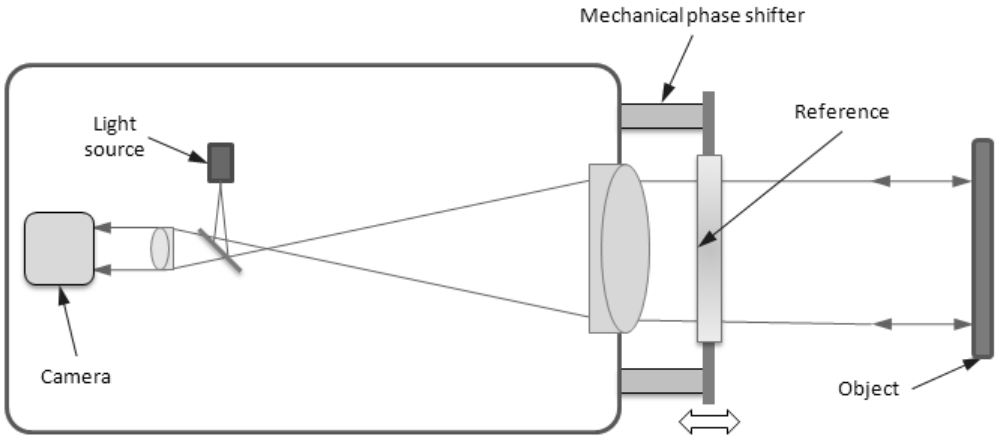

Figure 1: Laser Fizeau interferometer for optical testing, with mechanical phase shifting.

*peterd@zygo.com

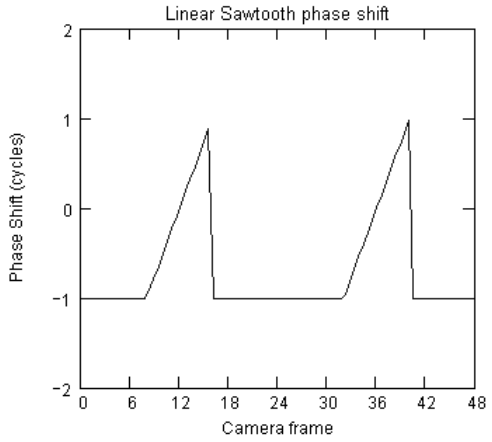

Figure 2: Common linear phase shift pattern for two successive measurements.

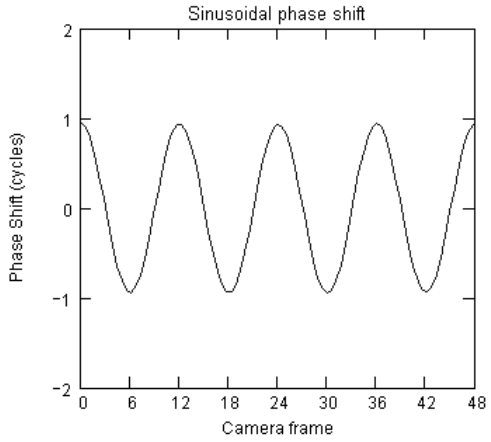

Figure 3: Continuous sinusoidal phase shifting.

Conventional linear phase shifting places high demands on the phase shifting mechanism, which must execute a linear motion, reverse direction, setup and repeat for the next measurement (Figure 2). This motion can be difficult to for a mechanical system while maintaining fidelity in the linear ramp, particularly if it is heavily loaded. One can readily imagine a triangular phase shift pattern or perhaps with rounded edges at the turnaround points to improve the situation. Best of all would be a purely sinusoidal phase shift, as in Figure 3. This more natural reciprocal motion is friendlier to mechanical systems and other methods of phase shifting that more easily support a single-frequency oscillatory motion.

Recognizing the advantage of a sinusoidal phase shift, Sasaki began a study of the technique in the 1980's, and introduced a four-frame demodulation algorithm having the same basic form as the linear four-frame algorithm popular at the time [2]. He went on to perform a random-noise error analysis [3] and to describe a sinusoidal Fizeau [4]. Over the years, several Researchers have proposed instruments based on sinusoidal phase shifting, without however dethroning the dominant linear techniques. With notable exceptions [5][6],there are few papers on sinusoidal phase shifting outside of Sasaki's Group, and commercial PSI systems rely exclusively on linear scans. Possible explanations include improvements in modulator design as well as significant advances in error-compensating linear PSI algorithms.

The primary goal of this document is to demonstrate that sinusoidal PSI or *SinPSI* can be as robust and computationally efficient as modern linear PSI. To this end, we provide new error-compensating SinPSI algorithms and the results of a new, comprehensive error analysis to close the gap between sinusoidal and linear PSI. The intent is to provide greater flexibility in methods of phase shifting in instrument design.

For brevity, this conference proceedings paper provides only the results of the mathematical development leading to the algorithms and error analysis. The derivations will be provided in an archival journal article to be published separately.

2. PHASE-SHIFTED INTERFERENCE SIGNAL

The central task of PSI is to determine a height h from the interference phase

$$\theta = 4\pi h/\lambda \tag{1}$$

at multiple positions in the field of view by evaluation of the interference intensity

$$I(\theta,t) = q\left\{1+V\cos\left[\theta+\phi(t)\right]\right\}. \tag{2}$$

To enable an accurate evaluation for unknown fringe visibility V and average intensity q, PSI prescribes a sequence of intensities $I_{1,2,3...}$ recorded over time t while shifting an offset phase $\phi(t)$. In traditional PSI, the phase shift is linear and generates a single-frequency tone having the phase offset θ that we seek. As examples, the following widely-used 4- and 5-frame algorithms use a phase shift increment of $\pi/2$:

$$\tan(\theta) = \frac{I_3 - I_1}{I_0 - I_2} \tag{3}$$

$$\tan(\theta) = \frac{2(I_3 - I_1)}{(I_0 + I_4) - 2I_2}, \tag{4}$$

while the following 13-frame algorithm uses a frame increment of $\pi/4$:

$$\tan(\theta) = \frac{-4(I_1 + I_{11}) - 12(I_2 + I_{10} + I_3 + I_9) + 16(I_5 + I_7) + 24I_6}{3(I_0 - I_{12}) + 4(I_1 - I_{11}) - 12(I_3 - I_9) - 21(I_4 - I_8) - 16(I_5 - I_7)}. \tag{5}$$

For SinPSI, we define the phase shift (Figure 3) as a cosine of amplitude u:

$$\phi(t) = u\cos\left[\alpha(t)\right]. \tag{6}$$

The linear, time-dependent phase of the shift is $\alpha(t) = 2\pi ft$ where f is the frequency e.g. in Hz. The time dependence for α will be implicit in all of the equations that follow.

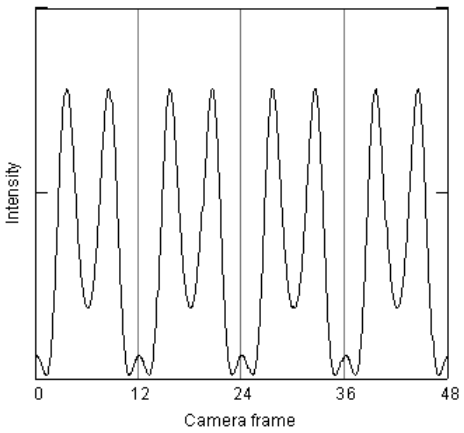

Figure 4: Interference intensity pattern for the sinusoidal phase shift shown in Figure 3.

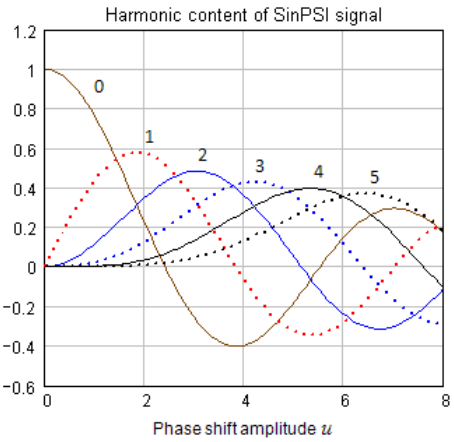

Figure 5: Strength of even (solid lines) and odd (dashed lines) harmonics in the SinPSI signal.

The mathematical consequence of the sinusoidal phase shift of Eq.(6) is an expansion of Eq.(2) to a sum of harmonics (Figure 4 and Figure 5) weighted by Bessel functions J_ν:

$$I(\theta,\alpha) = qD(\theta) + qV\cos(\theta)C(\alpha) + qV\sin(\theta)S(\alpha) \tag{7}$$

where

$$D(\theta) = 1 + VJ_0(u)\cos(\theta) \tag{8}$$

$$S(\alpha) = 2\sum_{\nu=1,3,5...}^{\infty}(-1)^{(\nu+1)/2}J_\nu(u)\cos(\nu\alpha) \tag{9}$$

$$C(\alpha) = 2\sum_{\nu=2,4,6...}^{\infty}(-1)^{\nu/2}J_\nu(u)\cos(\nu\alpha) \tag{10}$$

.

The phases of these harmonics are independent of the interference phase, thus unlike linear phase shifting, we do not determine θ by a Fourier phase analysis. Rather, in SinPSI, we note that the strengths of the odd harmonics $S(\alpha)$ are proportional to the sine of θ and the strengths of the even harmonics $C(\alpha)$ are proportional to the cosine of θ. Comparing the relative strengths of the odd and even harmonics provides quadrature values for θ.

3. SinPSI ALGORITHM DESIGN

Let us define a sequence of P phases α_j of the sinusoidal phase shift starting at an offset phase φ and spaced by $\Delta\alpha$:

$$\alpha_j = j\Delta\alpha + \varphi \tag{11}$$

$$j = 0,1,2..P-1. \tag{12}$$

The corresponding intensities form a vector I_j. Now define algorithm vectors $(h_{odd})_j$, $(h_{even})_j$ such that the dot product of these vectors and the intensities I_j tells us the strength of the odd and even harmonics, respectively:

$$\tan(\theta) = \frac{\Gamma_{even}}{\Gamma_{odd}}\frac{\sum_j (h_{odd})_j I_j}{\sum_j (h_{even})_j I_j}. \tag{13}$$

A detailed analysis shows that the constant normalizing factors in Eq.(13) are

$$\Gamma_{odd} = 2 \sum_{\nu=1,3,5...}^{\infty} (-1)^{(\nu+1)/2} J_\nu(u) B(\nu) Q_{odd}(\nu) \tag{14}$$

$$\Gamma_{even} = 2 \sum_{\nu=2,4,6...}^{\infty} (-1)^{\nu/2} J_\nu(u) B(\nu) Q_{even}(\nu) \tag{15}$$

where

$$Q_{odd}(\nu) = \sum_j (h_{odd})_j \cos(\nu\alpha_j) \tag{16}$$

$$Q_{even}(\nu) = \sum_j (h_{even})_j \cos(\nu\alpha_j) \tag{17}$$

,

and where the effect of camera frame integration is

$$B(\nu) = \frac{\sin(\nu\Delta\alpha/2)}{\nu\Delta\alpha/2}. \tag{18}$$

As shown in Eq.(13), SinPSI algorithms are similar in form to that of linear PSI algorithms—i.e., the arctangent of the ratio of a weighted sum of intensity values acquired sequentially during the phase shift. However, the principles of good algorithm design differ significantly from conventional linear phase shifting and established optimization techniques do not apply. Good SinPSI algorithm design centers on developing coefficient vectors that keep the ratio of the normalization constants in Eq.(14) and Eq.(15) stable in the presence of disturbances such as errors in the phase shift excursion. In part this involves constructing coefficient vectors so that if one of the harmonics is altered by a disturbance it is naturally balanced by an opposing change in another harmonic.[7]

4. EXAMPLE SinPSI ALGORITHMS

As a point of reference, we present a first example SinPSI algorithm similar to that of Sasaki, and having the merit of requiring only 4 camera frames of intensity data. This algorithm has a phase increment $\Delta\alpha = \pi/2$, a starting offset phase $\varphi = 0$, and a nominal phase shift amplitude $u = 2.45$:

$$\boxed{\tan(\theta) = \frac{1.4176(-I_0 + I_2)}{-I_0 + I_1 - I_2 + I_3}}. \tag{19}$$

The 4-frame algorithm does not fall in the class of error-compensating algorithms because the normalization ratio $\Gamma_{even}/\Gamma_{odd}$ calculated from Eq.(14) and Eq.(15) is unstable with phase shift amplitude u .

A first example error-compensating 8-frame SinPSI algorithm has a phase increment $\Delta\alpha = \pi/4$, a starting offset phase $\varphi = \pi/8$, and nominal phase shift amplitude $u = 2.93$:

$$\tan(\theta) = \frac{-1.6647(I_1 - I_2 - I_5 + I_6)}{-(I_0 + I_3 + I_4 + I_7) + (I_1 + I_2 + I_5 + I_6)} \tag{20}$$

A second example of an error-compensating SinPSI algorithm uses 12-frames, has a phase increment $\Delta\alpha = \pi/6$, a starting offset phase $\varphi = \pi/12$ and nominal phase shift amplitude $u = 3.517$:

$$\tan(\theta) = \frac{1.2461(I_0 - I_5 - I_6 + I_{11}) - 1.5525(I_1 - I_4 - I_7 + I_{10}) - 2.5746(I_2 - I_3 - I_8 + I_9)}{0.2707(I_0 + I_5 + I_6 + I_{11}) - 2.6459(I_1 + I_4 + I_7 + I_{10}) + 2.3753(I_2 + I_3 + I_8 + I_9)} \tag{21}$$

These example SinPSI algorithms have been designed with a high degree of symmetry, such that there are only a few independent values for the coefficients. They have also been designed to balance harmonics so that they are stable with variations in the phase shift amplitude u . They represent a class of SinPSI algorithms that compensate for the most common error sources in a way that compares well with traditional linear PSI algorithms.

5. ERROR ANALYSIS

5.1 Phase shift calibration

A classic performance criterion for PSI is sensitivity to deviations in the phase shift excursion from the expected or optimal value. Some of these variations are inevitable—in a high-NA spherical Fizeau cavity with a mechanical phase shifting mechanism, the phase shift excursion varies as a function of angle. In other cases, there is an uncertainty or variability in the calibration of the phase shift.

The effect of calibration on linear PSI is well understood and analytical formulas provide the measurement error as a function of calibration error [8]. Figure 6 shows these errors for the established 4-, 5- and 13-frame linear PSI algorithms provided in Eq.(3), Eq.(4) and Eq.(5).

In SinPSI, the standard deviation of the phase error ε from phase-shift calibration error δu is

$$\varepsilon_{stdv}(\delta u) = \frac{1}{2\sqrt{2}} \left| \rho(\delta u) - 1 \right| \tag{22}$$

where

$$\rho(\delta u) = \frac{\Gamma_{even}(u + \delta u)}{\Gamma_{odd}(u + \delta u)} \frac{\Gamma_{odd}}{\Gamma_{even}} . \tag{23}$$

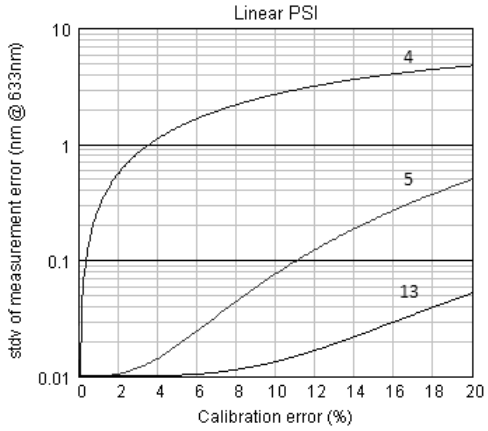

Figure 6: Measurement error in nm rms at 633nm wavelength for the 4-, 5- and 13-frame linear PSI algorithms as a function of calibration error

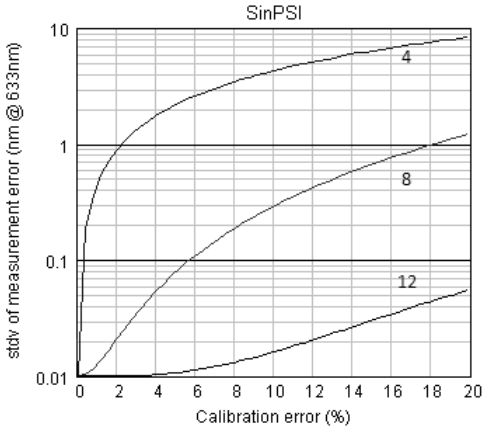

Figure 7: Measurement error in nm rms at 633nm wavelength for the 4-, 8- and 12-frame SinPSI algorithms as a function of calibration error.

The error is cyclic at twice the rate of θ, just as in linear phase shifting. Figure 7 shows that the results for SinPSI are comparable to those of conventional linear PSI.

5.2 Additive random noise

Random noise changes the interference intensity signal from Eq.(2) to

$$I(\theta,t) = q\left\{1+V\cos\left[\theta+\phi(t)\right]\right\}+n(\sigma,t), \tag{24}$$

where σ is the rms of the random noise $n(\sigma,t)$. A mathematical analysis of additive random noise for SinPSI leads to the following formula for the rms phase error:

$$\varepsilon_{rms} = \left(\frac{\sigma}{qV}\right)\frac{1}{\sqrt{2}}\sqrt{\left(\frac{p_{even}}{\Gamma_{even}}\right)^2+\left(\frac{p_{odd}}{\Gamma_{odd}}\right)^2} \tag{25}$$

where

$$p_{odd} = \sqrt{\sum_j \left(h_{odd}\right)_j^2} \tag{26}$$

$$p_{even} = \sqrt{\sum_j \left(h_{even}\right)_j^2}\ . \tag{27}$$

A similar formula can be derived for the case of linear PSI. The summary results of Table 1 tell us the expected rms phase error ε_{rms} for an rms noise level σ/qV. The tabulated results are scaled by $633\,\text{nm}/4\pi$. As expected, the

sensitivity to noise declines with the number of camera frames, approximately at the rate of the square root of the number of frames. The comparison of SinPSI to linear PSI shows no appreciable differences.

Table 1: The rms error in nm for a 633-nm light source for an rms random noise level of 1% of the signal amplitude.

	error (nm)
SinPSI 4	0.45
SinPSI 8	0.32
SinPSI 12	0.29

	error (nm)
Linear 4	0.40
Linear 5	0.37
Linear 13	0.23

5.3 Multiplicative noise

Typical contributors to multiplicative noise include random and synchronous light source fluctuations. Multiplicative noise changes the value of q in Eq.(2). For a pure, single-frequency noise, the intensity modifies to

$$I(\theta,\alpha,\nu') = \left[q + n(\alpha,\nu')\right]\left\{1 + V\cos\left[\theta + \phi(\alpha)\right]\right\} \tag{28}$$

where for a frequency ν, rms σ and phase ξ, the noise is

$$n(\alpha,\nu') = \sqrt{2}\sigma\cos\left[\nu'\alpha + \xi\right]. \tag{29}$$

We have derived the mathematical solution to the error analysis problem for noise levels of a few percent or less. First define the functions for the odd harmonics

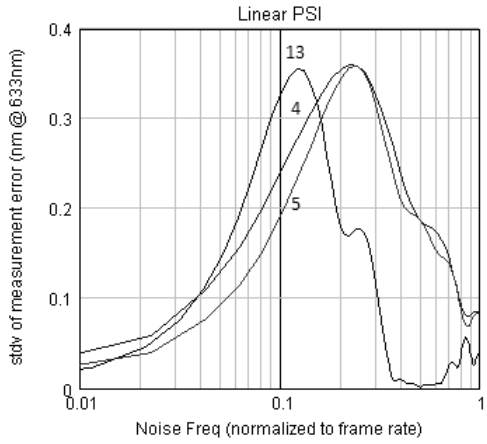

Figure 8: Multiplicative noise sensitivity for linear PSI. Measurement error in nm standard deviation at 633nm wavelength as a function of noise frequency, for an rms noise level of 1% of the signal strength.

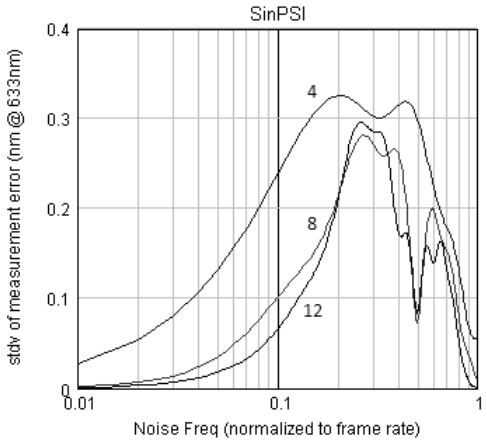

Figure 9: Multiplicative noise sensitivity for SinPSI. Measurement error in nm standard deviation at 633nm wavelength as a function of noise frequency, for an rms noise level of 1% of the signal strength.

$$N_{odd}\left(\nu'\right)=B\left(\nu'\right)\sum_{j}\left(h_{odd}\right)_{j}\cos\left(\nu'\alpha_{j}+\xi\right) \tag{30}$$

$$\Sigma_{1}^{odd}\left(\nu'\right)=\sum_{\nu=1,3,5...}^{\infty}\left(-1\right)^{\left(\nu+1\right)/2}J_{\nu}\left(u\right)\left[N_{odd}\left(\nu'-\nu\right)+N_{odd}\left(\nu'+\nu\right)\right] \tag{31}$$

$$\Sigma_{2}^{odd}\left(\nu'\right)=\sum_{\nu=2,4,6...}^{\infty}\left(-1\right)^{\nu/2}J_{\nu}\left(u\right)\left[N_{odd}\left(\nu'-\nu\right)+N_{odd}\left(\nu'+\nu\right)\right] \tag{32}$$

and similar equations for the even harmonics. Then the formula for multiplicative errors in SinPSI is

$$\varepsilon_{stdv}\left(\nu'\right)=\sqrt{\varepsilon_{rms}^{2}-\left\langle\varepsilon\right\rangle^{2}} \tag{33}$$

where the rms error is

$$\begin{aligned}\frac{\varepsilon_{rms}^{2}}{\left(\sigma/q\right)^{2}}&=\frac{4N_{odd}^{2}/V^{2}+\left(\Sigma_{1}^{odd}\right)^{2}+3\left(J_{0}N_{odd}+\Sigma_{2}^{odd}\right)^{2}}{4\Gamma_{odd}^{2}}\\&+\frac{4N_{even}^{2}/V^{2}+3\left(\Sigma_{1}^{even}\right)^{2}+\left(J_{0}N_{even}+\Sigma_{2}^{even}\right)^{2}}{4\Gamma_{even}^{2}}\\&-\frac{\Sigma_{1}^{odd}\left(J_{0}N_{even}+\Sigma_{2}^{even}\right)+\Sigma_{1}^{even}\left(J_{0}N_{odd}+\Sigma_{2}^{odd}\right)}{2\Gamma_{odd}\Gamma_{even}}\end{aligned} \tag{34}$$

and the mean error (or error offset independent of θ) is

$$\left\langle\varepsilon\right\rangle=\frac{\sigma}{q\sqrt{2}}\left(\frac{J_{0}\,N_{odd}}{\Gamma_{odd}}-\frac{\Sigma_{1}^{even}}{\Gamma_{even}}+\frac{\Sigma_{2}^{odd}}{\Gamma_{odd}}\right). \tag{35}$$

There is an implicit dependence on the noise phase from Eq.(30), so Figure 9 shows noise sensitivity for the 4-, 8- and 12-frame SinPSI algorithms calculated as the square root of the sum of the squares for two noise phases ξ =0 deg and ξ =90 deg. Figure 8 shows the results of a similar analysis for the 4-, 5- and 13-frame linear PSI methods. In linear PSI, the peak sensitivity is given by the frequency of the interference signal itself, which is 1/4 the camera rate for the 4- and 5-frame algorithms and 1/8 the camera rate for the 13-frame algorithm. In the case of SinPSI, even though the sampling is progressively slower with increasing numbers of frames, the longer algorithms operate at higher harmonics and therefore the peak sensitivity remains at higher frequencies. We can conclude that there are no special problems with SinPSI when compared to linear PSI for multiplicative noise and that SinPSI may even present some advantages at low frequencies for the 8- and 12-frame error-compensating algorithms.

5.4 Vibration

Because the data acquisition takes place over time, sensitivity to vibration is a major issue for PSI. The sensitivity as a function of vibrational frequency for linear PSI has been previously derived [9] and Figure 10 shows the results for the example algorithms from in Eq.(3), Eq.(4) and Eq.(5). The peak sensitivity is at 1/2 the camera rate for the 4- and 5-frame algorithms and 1/4 the camera rate for the 13-frame algorithm.

The formula for the standard deviation $\varepsilon_{stdv}(\nu')$ of vibration-induced errors in SinPSI uses the same definitions Eq.(30), Eq.(31), Eq.(32) and Eq.(33); where the rms error is now

$$\frac{\langle \varepsilon^2 \rangle_\theta}{\sigma^2} = \frac{\left(J_0\, N_{odd} + \Sigma_2^{odd}\right)^2 + 3\left(\Sigma_1^{odd}\right)^2}{4\Gamma_{odd}^2} + \frac{3\left(J_0\, N_{even} + \Sigma_2^{even}\right)^2 + \left(\Sigma_1^{even}\right)^2}{4\Gamma_{even}^2} + \frac{\Sigma_1^{odd}\left(J_0 N_{even} + \Sigma_2^{even}\right) + \Sigma_1^{even}\left(J_0\, N_{odd} + \Sigma_2^{odd}\right)}{2\Gamma_{odd}\Gamma_{even}} \tag{36}$$

the mean error (or error offset independent of θ) is

$$\langle \varepsilon \rangle = \frac{\sigma}{\sqrt{2}}\left(\frac{J_0\, N_{even}}{\Gamma_{even}} + \frac{\Sigma_1^{odd}}{\Gamma_{odd}} + \frac{\Sigma_2^{even}}{\Gamma_{even}}\right) \quad . \tag{37}$$

and the standard deviation σ of the vibrational noise is in units of radians. Figure 11 shows that the simple 4-frame SinPSI algorithm has a higher sensitivity to vibration when compared to the 4-frame linear PSI algorithm; however, the 8- and 12-frame error-compensating SinPSI algorithms show performance comparable to the 5- and 13-frame linear PSI methods. From this we conclude once again that SinPSI does not present any special problems for vibration sensitivity provided that we use more than 4 camera frames.

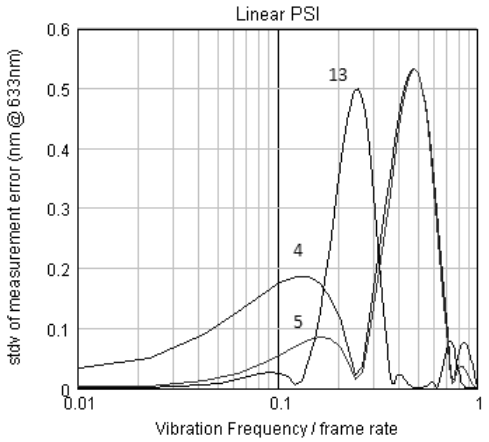

Figure 10: Sensitivity to vibration for linear PSI. Measurement error in nm standard deviation at 633nm wavelength as a function of vibrational frequency, for an rms vibration of 1nm.

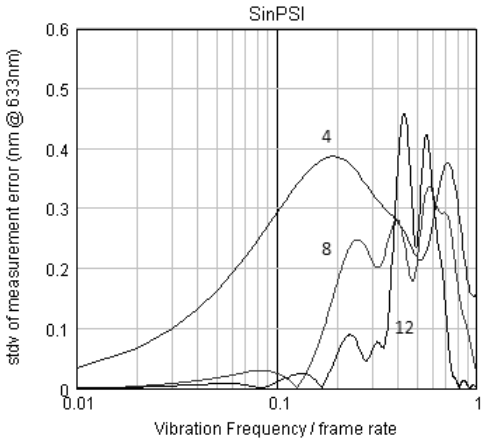

Figure 11: Sensitivity to vibration for SinPSI. Measurement error in nm standard deviation at 633nm wavelength as a function of vibrational frequency, for an rms vibration of 1nm.

5.5 Detector nonlinearity

A nonlinearity of order $n \geq 2$ of a detector or camera may be defined by

$$\Delta I = q\zeta\left[\left(\frac{I-q}{q}\right)^2 - \frac{1}{2}\right]\left(\frac{I-q}{q}\right)^{(n-2)} \qquad (38)$$

where ΔI refers to the deviation with respect to a linear fit to the detected signal I, and q is the mean intensity. Figure 12 illustrates a quadratic nonlinearity. Note that ζ is the peak-valley (P-V) departure from linear over the full dynamic range of the detector.

Detector nonlinearity is a particularly complex error source in SinPSI, generating a large spectrum of harmonics. The results in Table 2 for both linear PSI and SinPSI are for a numerical simulation.

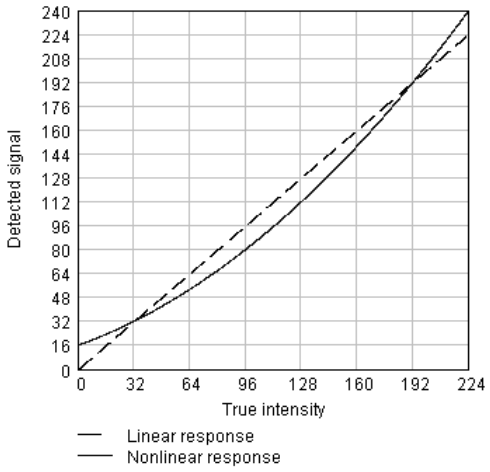

Figure 12: Quadratic detector nonlinearity ζ of 29% P-V over a full range of 256 grey levels.

From Table 2 we conclude that linear PSI has an advantage with respect to SinPSI when considering detector nonlinearity. This is not a large source of concern for most detectors, given that the nonlinearity is usually better than <1%; but could be an issue e.g. with CMOS cameras. Detector nonlinearity in SinPSI can in theory generate ripple error at 4 times the fringe frequency; therefore, an effective strategy for suppressing these errors may be to average at least two acquisitions with an overall phase offset of ¼ of a fringe between them.

Table 2: Sensitivity to detector nonlinearity of order n, expressed as the standard deviation in nm at 633nm for a nonlinearity of 1% P-V.

	$n=2$	$n=3$	$n=4$	average
SinPSI 4	0.22	0.13	0.17	0.17
SinPSI 8	0.17	0.11	0.12	0.13
SinPSI 12	0.03	0.15	0.13	0.10
Linear 4	0.00	0.10	0.00	0.03
Linear 5	0.00	0.10	0.07	0.06
Linear 13	0.00	0.00	0.00	0.00

5.6 Phase shift nonlinearity

Although a sinusoid should in principle be easier to manage than a linear scan for most phase shifting mechanisms, there is nonetheless a possibility for nonlinear response, e.g. with a heavily-loaded mechanical phase shifter or low-voltage piezo actuator. Common imperfections include quadratic and cubic nonlinearities, as illustrated in Figure 13 and Figure 14, respectively.

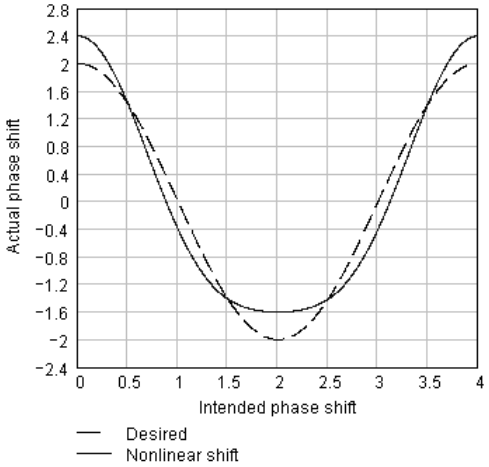

Figure 13: Sinusoidal phase shift with a quadratic nonlinearity ζ of 40% P-V.

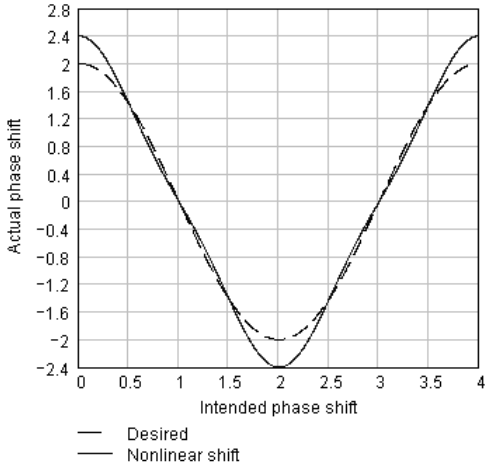

Figure 14: Sinusoidal phase shift with a 3rd-order nonlinearity ζ of 40% P-V.

Similarly to Eq.(38), a nonlinear phase shift may be written as a polynomial of order $n \geq 2$ using

$$\Delta\phi = u\zeta\left[\left(\frac{\phi - \langle\phi\rangle}{u}\right)^2 - \frac{1}{2}\right]\left(\frac{\phi - \langle\phi\rangle}{u}\right)^{(n-2)} \tag{39}$$

where $\Delta\phi$ refers to the deviation with respect to a linear fit to the desired phase shift ϕ, $\langle\phi\rangle$ is the mean phase and u is the phase shift amplitude. The results of numerical calculations for phase-shift nonlinearity in Table 3 shows an advantage of approximately a factor of two for linear PSI; but this advantage is not significant for the longer algorithms—both 12-frame SinPSI and 13-frame linear PSI show high tolerance for phase shifting errors.

Table 3: Sensitivity to phase-shift nonlinearity of order n, expressed as the standard deviation in nm at 633nm for a nonlinearity of 1% P-V.

	$n = 2$	$n = 3$	$n = 4$	average
SinPSI 4	0.14	0.22	0.04	0.13
SinPSI 8	0.19	0.12	0.13	0.15
SinPSI 12	0.01	0.04	0.02	0.02
Linear 4	0.04	0.10	0.05	0.06
Linear 5	0.11	0.02	0.08	0.07
Linear 13	0.00	0.02	0.01	0.01

5.7 Phase shift timing error

SinPSI has some error considerations that do not appear at all in linear PSI. In this section, we consider the importance of synchronizing the data acquisition with the starting point for the sinusoidal phase shift. This is not a requirement in linear PSI—we can begin to grab camera frames anytime during the linear phase shift and the profile results, apart from an overall offset, do not change. The original Sasaki SinPSI algorithm introduced in 1989 had a slightly alarming sensitivity to phase shift timing, requiring a synchronization of <1.5 degree to maintain a standard deviation of <1nm [6]. One goal of the present work was to relax this requirement.

To calculate the effect of timing error, first redefine Eq.(14) through Eq.(17) for an unintended phase offset $\delta\varphi$:

$$\Gamma_{odd}\left(\delta\varphi\right) = 2\sum_{\nu=1,3,5...}^{\infty}\left(-1\right)^{(\nu+1)/2} J_{\nu}\left(u\right) B\left(\nu\right) Q_{odd}\left(\nu,\delta\varphi\right) \tag{40}$$

$$\Gamma_{even}\left(\delta\varphi\right) = 2\sum_{\nu=2,4,6...}^{\infty}\left(-1\right)^{\nu/2} J_{\nu}\left(u\right) B\left(\nu\right) Q_{even}\left(\nu,\delta\varphi\right) \tag{41}$$

where now

$$Q_{odd}\left(\nu,\delta\varphi\right) = \sum_{j}\left(h_{odd}\right)_{j}\cos\left[\nu\left(\alpha_{j}+\delta\varphi\right)\right] \tag{42}$$

$$Q_{even}\left(\nu,\delta\varphi\right) = \sum_{j}\left(h_{even}\right)_{j}\cos\left[\nu\left(\alpha_{j}+\delta\varphi\right)\right]. \tag{43}$$

The standard deviation of the measurement phase error is then

$$\varepsilon_{stdv} = \frac{1}{2\sqrt{2}}\left|\,\rho\left(\delta\varphi\right)-1\,\right| \tag{44}$$

$$\rho = \frac{\Gamma_{even}\left(\delta\varphi\right)}{\Gamma_{odd}\left(\delta\varphi\right)}\frac{\Gamma_{odd}}{\Gamma_{even}}, \tag{45}$$

where $\Gamma_{odd}, \Gamma_{even}$ are the normalizing coefficients for the case where there is no timing error.

The results in Figure 15 show that for the algorithms defined in this paper, timing error is not a critical issue. The 4-frame algorithm has significantly reduced sensitivity when compared to Sasaki's original algorithm, and the 12-frame algorithm has <0.1nm error with as much as 16 deg of timing offset.

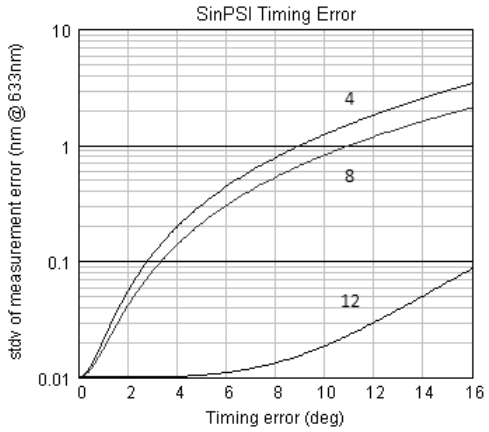

Figure 15: Effect of a timing error between the beginning of the sinusoidal phase shift and the camera trigger for SinPSI.

6. CONCLUSIONS

The new algorithms and error analysis in this paper have shown that SinPSI can provide competitive performance to traditional linear PSI while enjoying the benefits of the less demanding sinusoidal mechanical scan. The computational burden is no higher, and the algorithm performance is equivalent or better than for linear phase shifting, provided that modest measures are taken to control detector nonlinearity and synchronize the data acquisition with the sinusoidal phase shifting cycle.

We conclude from this study that SinPSI is a viable and useful alternative phase-shifting strategy for a variety of applications from optical testing to interference microscopy, and is of particular interest where the measurement performance is limited by the characteristics of the phase shifting mechanism. The next step in our on-going research will be to integrate the sinusoidal drive in a complete system with appropriate software for experimental evaluation.

REFERENCES

[1] D.Malacara, M. Servin, Z. Malacara, Interferogram Analysis for Optical Testing, 169-245 (1998).

[2] O. Sasaki, H. Okazaki, and M. Sakai, "Sinusoidal phase modulating interferometer using the integrating-bucket method," Appl. Opt. 26, 1089 (1987).

[3] O. Sasaki and H. Okazaki, "Analysis of measurement accuracy in sinusoidal phase modulating interferometry," Appl. Opt. 25, 3152 (1986).

[4] O. Sasaki, T. Okamura, and T. Nakamura, "Sinusoidal phase modulating Fizeau interferometer," Appl. Opt. 29, 512 (1990).

[5] C. Zhang and X. Wang, “Sinusoidal phase-modulating laser diode interferometer for measuring angular displacement,” Opt. Eng. 43, 3008 (2004).

[6] A. Dubois, "Phase-map measurements by interferometry with sinusoidal phase modulation and four integrating buckets ," J. Opt. Soc. Am. A 18, 1972 (2001).

[7] US and Foreign patents pending, assigned to Zygo Corporation.

[8] P. de Groot, "Phase-shift calibration errors in interferometers with spherical Fizeau cavities," Appl. Opt. 34, 2856 (1995).

[9] P. de Groot, "Vibration in phase shifting interferometry," J. Opt. Soc. Am. A 12, 354 (1995).